ELSEVIER

International Journal of Heat and Fluid Flow 21 (2000) 526–534

International Journal of HEAT AND FLUID FLOW

www.elsevier.com/locate/ijhff

# Direct numerical simulation for laminarization of turbulent forced gas flows in circular tubes with strong heating

Shin-ichi Satake [a,*], Tomoaki Kunugi [b], A. Mohsen Shehata [c], Donald M. McEligot [d,e]

[a] *Department of Mechanical System Engineering, Toyama University, Toyama 930-8555, Japan*
[b] *Department of Nuclear Engineering, Kyoto University, Yoshida, Sakyo, Kyoto 606-8501, Japan*
[c] *Xerox Corporation, 800 Phillips Road, 111–20N, Webster, NY 14580, USA*
[d] *Idaho National Engineering and Environmental Laboratory, Idaho Falls, ID 83415-3885, USA*
[e] *University of Arizona, Tucson, AZ 85721, USA*

**Abstract**

The direct numerical simulation (DNS) of turbulent transport for a gas with variable properties has been conducted to grasp and understand the laminarization phenomena caused by strong heating. In this study, the inlet Reynolds number based on a bulk velocity and pipe diameter was taken as $Re = 4300$ as in the experiments by Shehata and McEligot (1998). The measured wall temperature distribution was applied as a thermal boundary condition. The number of computational nodes used in the heated region was $768 \times 64 \times 128$ in the $z$-, $r$- and $\phi$-directions, respectively. Turbulent quantities, such as the mean flow, temperature fluctuations, turbulent stresses and the turbulent statistics, were obtained via DNS. Predicted mean velocity and temperature distributions and integral parameters agreed well with the experiments. The Reynolds shear stress, indicating turbulent transport of momentum, decreases along the streamwise direction. The cause of this reduction can be considered to be that the fluid behavior changes drastically in the near wall region due to strong heating which induces significant variations of the gas properties and, in turn, acceleration and buoyancy effects. In a visualization of the results, one sees that the vortical structures are primarily suppressed within the first section of the heated region ($z/D = 0$–5) and are not regenerated further downstream. 

*Keywords:* Laminarization; Heat transfer; Turbulent flow; Tube; Gas property variation

## 1. Introduction

General effects of strong heating of a gas are variation of the transport properties, reduction of density causing acceleration of the flow in the central core, and – in some cases – significant buoyancy forces. Growth of the internal thermal boundary layer leads to readjustment of any previously fully developed turbulent momentum profile. No truly fully established conditions are reached because the temperature rises – leading, in turn, to continuous axial and radial variation of properties such as the gas viscosity. In an application such as the high temperature engineering test reactor (HTTR) in Japan (or reduction of flow scenarios in other plants) another complication arises. To obtain high outlet temperatures, design gas flow rates are kept relatively low. For example, at the exit of the HTTR cooling channels, the Reynolds number is about 3500 (Takase et al., 1990). In this range, the heat transfer parameters may appear to correspond to turbulent or laminar flow or to an intermediate behavior, depending on the heating rate (Bankston, 1970), with consequent differences in their magnitudes. The situation, where laminar values are measured at Reynolds numbers typifying turbulent flow is called "laminarization" by some authors. For further general background on laminarization in internal convective heat transfer to gases, a survey by McEligot (1986) may be useful.

For dominant forced convection with significant gas property variation, in low Mach number flow of common gases through a circular tube, until recently the only published profile data available to guide (or test) the development of predictive turbulence models apparently have been Perkin's measurements (1975) of mean temperature distributions. Further, direct numerical simulation (DNS) results have not been available for these conditions. Shehata and McEligot (1998) obtained the first mean velocity distributions for this situation. The few 'advanced' turbulence models applied for high heating rates (Kawamura, 1979; Fujii et al., 1991; Torii et al., 1993; Torii and Yang, 1997) were developed *without* the benefit of velocity and temperature distributions in strongly heated, dominant forced flow for guidance or testing. None of these investigators appear to have compared their predictions to internal data for strongly heated gas flows. To the authors' knowledge, the only

* Corresponding author. Tel.: +81-764-45-6887; fax: +81-764-45-6887.
*E-mail address:* ssatake@eng.toyama-u.ac.jp (S. Satake).

0142-727X/00/$ - see front matter 
PII: S0142-727X(00)00041-2

**Notation**

| | |
|---|---|
| $C_f$ | friction coefficient |
| $c_p$ | specific heat at constant pressure |
| $D$ | diameter |
| $g_c$ | units conversion factor, e.g., 1 kg m /(N s$^2$) |
| $g$ | acceleration of gravity |
| $k$ | turbulent kinetic energy |
| $h$ | heat transfer coefficient |
| $m$ | mass flow rate |
| $Nu$ | Nusselt number, $Nu = 2hR/\lambda$ |
| $P$ | pressure |
| $P^+$ | non-dimensional pressure drop, $\rho_{in} g_c (P_{in} - P)/G^2$ |
| $Pr$ | molecular Prandtl number |
| $q_0$ | wall heat flux |
| $R$ | radius |
| $Re_b$ | bulk Reynolds number, $Re_b = 2U_b R/v$ |
| $St$ | Stanton number, $St = Nu/Re_b Pr$ |
| $T$ | temperature |
| $U$ | mean velocity |
| $U_b$ | bulk mean velocity |
| $u_z,\ u_r,\ u_\phi$ | velocity components in the $z$, $r$ and $\phi$ directions |
| $u_\tau$ | friction velocity, $u_\tau = (\tau_w/\rho)^{1/2}$ |
| $z,\ r,\ \phi$ | streamwise, radial and circumferential coordinates |

*Greeks*

| | |
|---|---|
| $\lambda$ | thermal conductivity |
| $v$ | kinematic viscosity |
| $\rho$ | density |
| $\tau_w$ | wall shear stress |

*Subscripts*

| | |
|---|---|
| $()_b$ | evaluated at bulk temperature |
| $()_{in}$ | evaluated at start of heating |
| $()_{out}$ | evaluated at exit |
| $()_{rms}$ | root-mean-square value |
| $()_w$ | evaluated at wall surface |
| $()'$ | fluctuating component |
| $()^+$ | normalized by wall variables |

numerical studies of 'advanced' turbulence models for turbulent and laminarizing flows at high-heating rates that utilized internal data have been those of Mikielewicz (1994), Ezato et al. (1997) and Nishimura et al. (1997) which employed measurements from Shehata and McEligot (1998).

In the present study, DNS for turbulent pipe flow with strong heating has been accomplished by means of the finite volume method developed by Satake and Kunugi (1998a,b). The turbulent statistics for the mean velocity and integral parameters are predicted and compared with careful measurements (Shehata and McEligot, 1998) for the same conditions. Furthermore, also presented are predictions for the Reynolds normal and shear stresses, the budget of turbulent kinetic energy and turbulent structures, which could not be measured in the experiment.

## 2. Solution procedure

Cylindrical coordinates are employed with $z$, $r$ and $\phi$, in the streamwise, radial and circumferential directions, respectively, as shown in Fig. 1. Then the continuity, the momentum and scalar equations become

$$\frac{\partial \rho}{\partial t} + \frac{\partial \rho u_z}{\partial z} + \frac{1}{r}\frac{\partial \rho r u_r}{\partial r} + \frac{1}{r}\frac{\partial \rho u_\phi}{\partial \phi} = 0, \tag{1}$$

$$\rho\frac{\partial u_z}{\partial t} + \rho u_z \frac{\partial u_z}{\partial z} + \rho u_r \frac{\partial u_z}{\partial r} + \rho \frac{u_\phi}{r}\frac{\partial u_z}{\partial \phi} = -\frac{\partial p}{\partial z} + \left(\frac{\partial \tau_{zz}}{\partial z} + \frac{1}{r}\frac{\partial}{\partial r}(r\tau_{rz}) + \frac{1}{r}\frac{\partial \tau_{\phi z}}{\partial \phi}\right) - \rho g, \tag{2}$$

$$\rho\frac{\partial u_r}{\partial t} + \rho u_z \frac{\partial u_r}{\partial z} + \rho u_r \frac{\partial u_r}{\partial r} + \rho \frac{u_\phi}{r}\frac{\partial u_r}{\partial \phi} - \frac{\rho u_\phi^2}{r} = -\frac{\partial p}{\partial r} + \left(\frac{\partial \tau_{rz}}{\partial z} + \frac{1}{r}\frac{\partial}{\partial r}(r\tau_{rr}) + \frac{1}{r}\frac{\partial \tau_{r\phi}}{\partial \phi} - \frac{\tau_{\phi\phi}}{r}\right), \tag{3}$$

$$\rho\frac{\partial u_\phi}{\partial t} + \rho u_z \frac{\partial u_\phi}{\partial z} + \rho u_r \frac{\partial u_\phi}{\partial r} + \rho \frac{u_\phi}{r}\frac{\partial u_\phi}{\partial \phi} + \rho \frac{u_r u_\phi}{r} = -\frac{1}{r}\frac{\partial p}{\partial \phi} + \left(\frac{\partial \tau_{\phi z}}{\partial z} + \frac{1}{r^2}\frac{\partial}{\partial r}(r^2\tau_{r\phi}) + \frac{1}{r}\frac{\partial \tau_{\phi\phi}}{\partial \phi}\right), \tag{4}$$

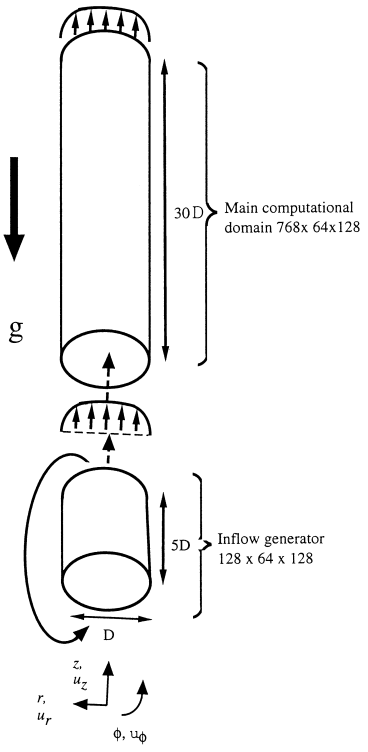


Fig. 1. Coordinate system and boundary conditions.

$$\rho C_p \frac{\partial T}{\partial t} + \rho C_p u_z \frac{\partial T}{\partial z} + \rho C_p u_r \frac{\partial T}{\partial r} + \rho C_p \frac{u_\phi}{r}\frac{\partial T}{\partial \phi} = \frac{\partial}{\partial z}\left(\lambda\frac{\partial T}{\partial z}\right) + \frac{1}{r}\frac{\partial}{\partial r}\left(r\lambda\frac{\partial T}{\partial r}\right) + \frac{1}{r}\frac{\partial}{\partial \phi}\left(\lambda\frac{1}{r}\frac{\partial T}{\partial \phi}\right), \tag{5}$$

where

$$\tau_{zz} = \mu\left[2\frac{\partial u_z}{\partial z} - \frac{2}{3}\nabla\cdot\mathbf{u}\right], \tag{6}$$

$$\tau_{rr} = \mu\left[2\frac{\partial u_r}{\partial r} - \frac{2}{3}\nabla\cdot\mathbf{u}\right], \tag{7}$$

$$\tau_{\phi\phi} = \mu\left[2\left(\frac{1}{r}\frac{\partial u_\phi}{\partial \phi} + \frac{u_r}{r}\right) - \frac{2}{3}\nabla\cdot\mathbf{u}\right], \tag{8}$$

$$\tau_{r\phi} = \tau_{\phi r} = \mu\left[r\frac{\partial}{\partial r}\left(\frac{u_\phi}{r}\right) + \frac{1}{r}\frac{\partial u_r}{\partial \phi}\right], \tag{9}$$

$$\tau_{\phi z} = \tau_{z\phi} = \mu\left[\frac{\partial u_\phi}{\partial z} + \frac{1}{r}\frac{\partial u_z}{\partial \phi}\right], \tag{10}$$

$$\tau_{zr} = \tau_{rz} = \mu\left[\frac{\partial u_z}{\partial r} + \frac{\partial u_r}{\partial z}\right], \tag{11}$$

$$\nabla\cdot\mathbf{u} = \frac{\partial u_z}{\partial z} + \frac{1}{r}\frac{\partial r u_r}{\partial r} + \frac{1}{r}\frac{\partial u_\phi}{\partial \phi}. \tag{12}$$

The DNS code with cylindrical coordinates can solve the continuity and momentum equations numerically using the radial momentum flux formulation. A second-order finite volume discretization scheme is applied to the spatial derivatives on a staggered mesh system in order to avoid a singularity at the center axis of the pipe (Verzicco and Orlandi, 1996). The low-Mach-number Navier–Stokes and continuity equations, formulated in cylindrical coordinates, are integrated in time by using the fractional-step method (Dukowicz and Dvinsky, 1992). As seen above, body force terms are included in the momentum equations to account for buoyancy effects. A second-order Crank–Nicholson scheme is applied to the terms in the radial direction and a modified third-order Runge–Kutta scheme (Spalart et al., 1991) is used for other terms. In our previous study regarding constant-property, turbulent pipe flow (Satake and Kunugi, 1998a,b), this DNS code has shown good agreement with the existing DNS results by Eggels (1994) and Akselvoll and Moin (1995).

## 3. Computational conditions

Air is the working fluid. Thermal properties are evaluated as power-law functions of the pointwise temperature and pressure with density estimated via the perfect gas approximation as by Perkins (1975) as follows:

Density

$$\rho = \rho_{\mathrm{ref}}\left(\frac{P}{P_{\mathrm{ref}}}\right)\left(\frac{T_{\mathrm{ref}}}{T}\right), \tag{13}$$

Viscosity

$$\mu = \mu_{\mathrm{ref}}\left(\frac{T}{T_{\mathrm{ref}}}\right)^{0.67}, \tag{14}$$

Specific heat at constant pressure

$$C_{\mathrm{p}} = C_{\mathrm{p,ref}}\left(\frac{T}{T_{\mathrm{ref}}}\right)^{0.095}, \tag{15}$$

Thermal conductivity

$$\lambda = \lambda_{\mathrm{ref}}\left(\frac{T}{T_{\mathrm{ref}}}\right)^{0.805}. \tag{16}$$

The subscript ref indicates that the value was taken at the reference state, typically at the gas inlet temperature and pressure (near 298 K and 0.09 MPa).

Uniform mesh spacing is applied to the circumferential ($\phi$) and the streamwise ($z$) directions, with $R^+\Delta\phi \approx 7.36$ and $\Delta_z^+ \approx 11.7$, respectively. In the radial direction($r$), a non-uniform grid of 64 nodes is employed with spacing specified by a hyperbolic tangent function. The computational domain consists of two parts, i.e., an inflow profile generator, which provides adiabatic, fully developed flow for the inlet to the heated region and a main part which corresponds to the heated region in the experiment. The number of computational nodes for the inflow generator is $128 \times 64 \times 128$ points in the $z$-, $r$- and $\phi$-directions, respectively.

The pipe length of the main part is approximately the same as in the experiment (Shehata and McEligot, 1998) shown in Fig. 1. The experimental data are provided as bases for comparison with the computational results. The inlet Reynolds number ($= U_{\mathrm{b}}D/\nu$) is assumed to be 4300; the conditions correspond to the Run 445 of the experiments. The number of grid points is $768 \times 64 \times 128$ in the $z$-, $r$- and $\phi$-directions, respectively. The inlet boundary condition is provided by the inflow generator; that is, a fully developed pipe flow with constant fluid properties is considered at the thermal entry. A convective boundary condition (Lowery et al., 1987) is imposed at the exit of the main computational domain. One should note that the mass balance between inflow and outflow must be maintained at every time step. This equality is obtained by multiplying the streamwise exit velocities at each radial point by the mass flow ratio ($m_{\mathrm{in}}/m_{\mathrm{out,calc}}$) after each step.

For the thermal boundary condition, the temperature distribution along the pipe wall was specified, based on the data. Although a constant heat flux was applied as the thermal boundary condition in the experiment, with the present DNS technique it is difficult to treat a constant wall heat flux condition for spatially developing flow problems (Satake and Kunugi, 1998c). Therefore, this DNS calculation is focused on the investigation of the turbulent heat and momentum transfer mechanisms in a pipe with a known wall temperature distribution, taken from the wall thermocouple measurements of Shehata and McEligot (1998).

## 4. Results and discussion

Predictions of integral quantities are considered first. Fig. 2 shows the relationship between the local Stanton number and the local bulk Reynolds number; dashed lines represent accepted correlations for the constant properties limit for turbulent and laminar flows ($Pr = 0.71$). The Reynolds number is 4300 at the inlet and, due to the increase of viscosity with temperature, decreases to about 3000 at the outlet, i.e., the

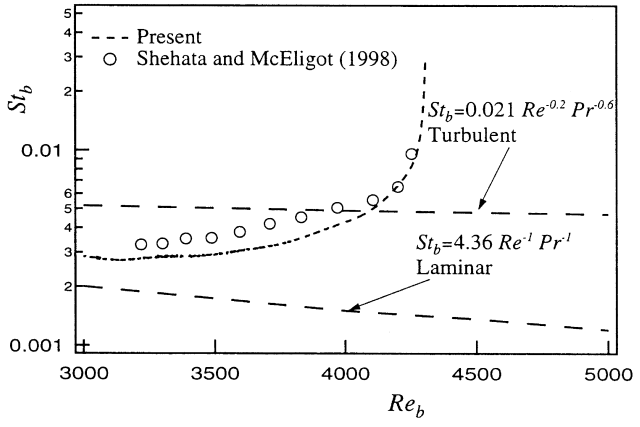


Fig. 2. The relationship between the local Stanton number and the local bulk Reynolds number.

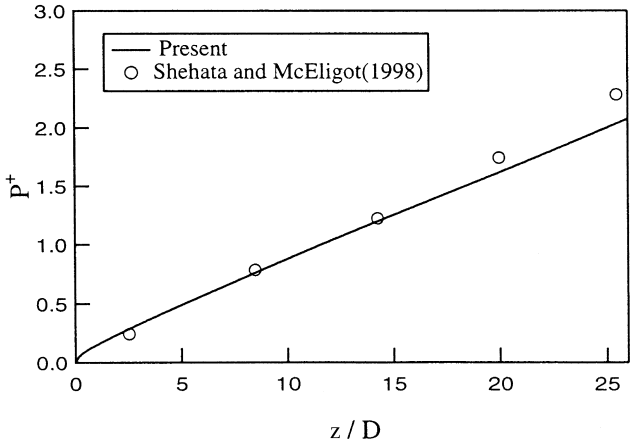


Fig. 3. Comparison of static pressure.

sequential axial data points pass from right to left on the plot. The non-dimensional static pressure drop is shown in Fig. 3. As noted by Ezato et al. (1997), the contributions to the pressure variation by the thermal energy addition, wall friction and vertical elevation change are in the approximate ratios 4:5:5 for this run (circle symbols). In the experiment the wall heat flux is controlled and, in data reduction, the local bulk temperature is determined from the deduced local wall heat flux. But, in the DNS calculation, local bulk temperature is obtained by integration of the local density, velocity and temperature profiles, which have been predicted from a specified wall-temperature variation from the experimental data of Shehata and McEligot (1998). Consequently, comparison of the predicted and measured bulk temperatures provides a measure of the consistency between the thermal boundary conditions in the simulation and in the experiment. This comparison is presented in Fig. 4. Overall, the agreements can be considered quite good for these three integral parameters, providing confidence in the capabilities of this DNS technique.

Figs. 5(a)–(c) present the comparisons of mean axial velocity profiles normalized by local bulk velocity. The comparisons are made at three representative locations, $z/D = 3.2$, $z/D = 14.2$ and $z/D = 24.5$, and show mostly excellent agreement with the exception of a few points near the wall at the first station, the most difficult measuring region (Shehata and McEligot, 1998). At the first station, the profile is characteristic of a turbulent pipe flow and there is an apparent

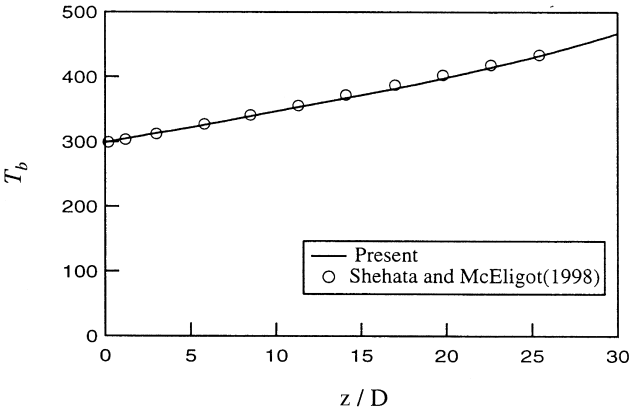


Fig. 4. The bulk temperature.

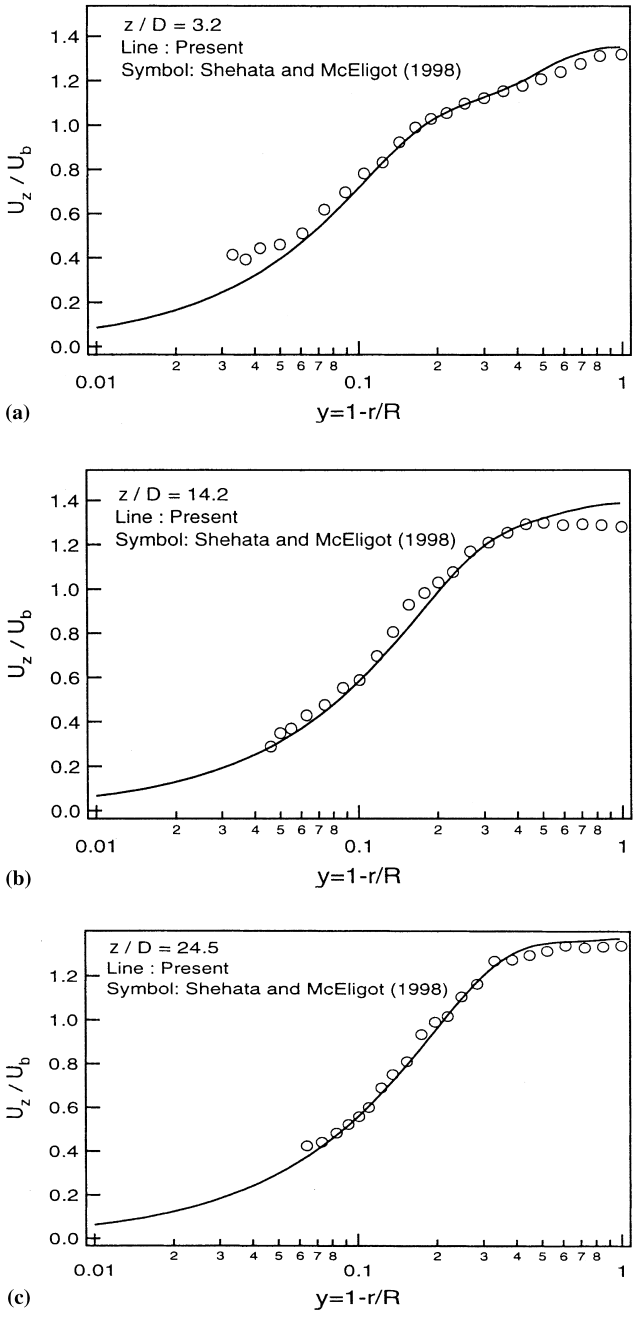


Fig. 5. Mean velocity profiles.

logarithmic section. The second station, about halfway along the heated section, already yields a mean velocity profile that is reminiscent of a laminar flow (e.g., a parabola or a Blasius profile when presented with semi-logarithmic coordinates). Results at the last station are comparable to those at the second. The excellent agreement throughout gives further confidence in the present DNS approach. Since it was not feasible to measure the fluctuating components or higher order statistics, this confidence is desirable as the remainder of this paper extends the DNS results to statistics for which there are no measurements available for comparison.

The distributions of mean temperature and temperature fluctuations are presented in Figs. 6 and 7. The mean-temperature profiles indicate the magnitudes of the property

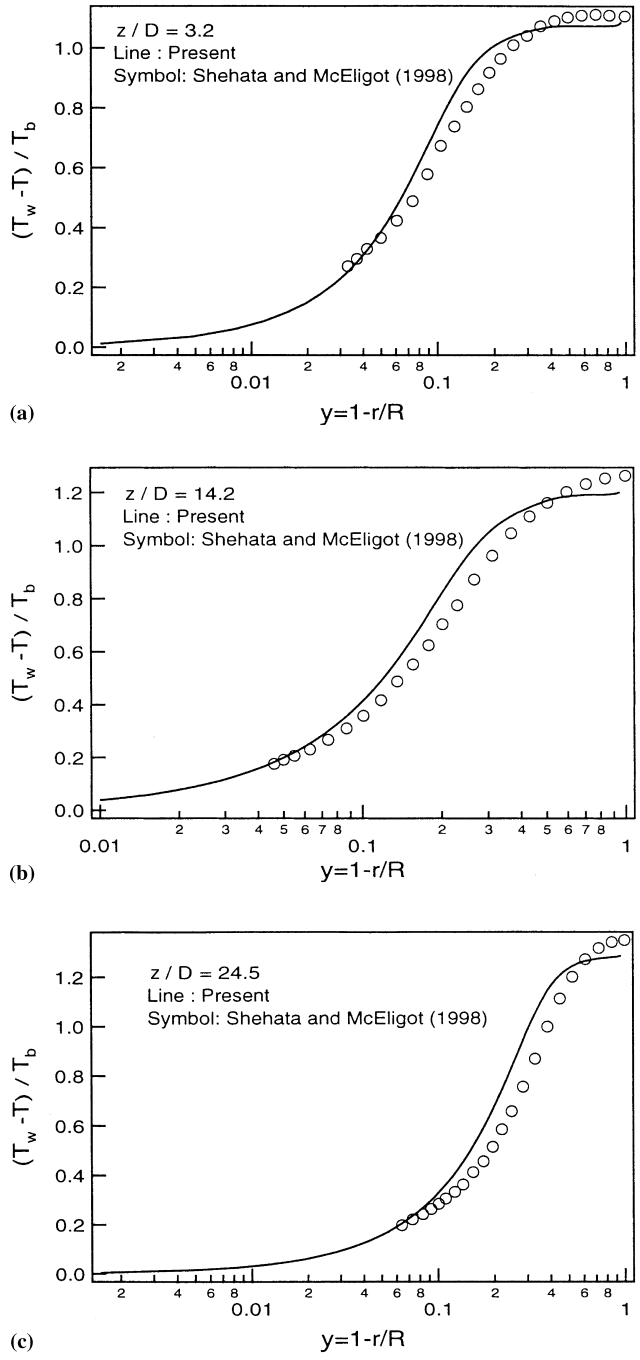


Fig. 6. Mean temperature profiles.

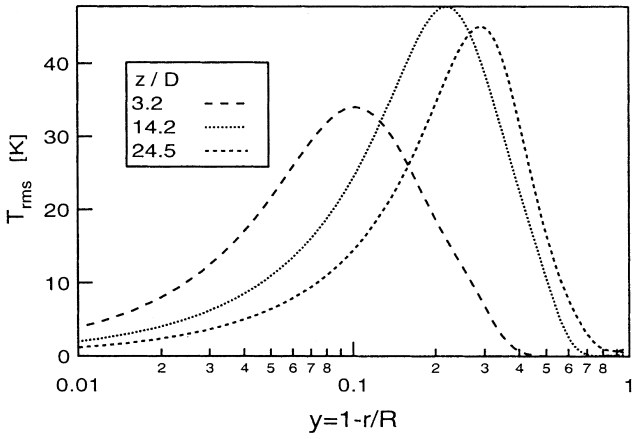


Fig. 7. Temperature fluctuation profiles.

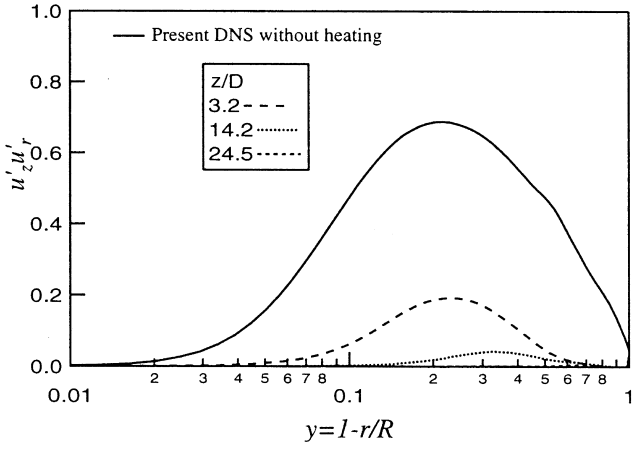


Fig. 8. Reynolds shear stress profiles.

variation across the tube since, as approximations, the properties can be considered to be power laws of the absolute temperature (density being related inversely). Likewise, the bulk temperature in Fig. 4 showed the variation along the tube. The successive profiles show the growth of the thermal boundary layer towards the centerline; it is predicted to be less rapid than observed with the temperature measurements. Near the wall the agreement is good so the predicted heat transfer coefficient is expected to be reasonable (as it is, e.g., Fig. 2). At the first station ($z/D = 3$), the peak in the fluctuation profile is near the wall; then it moves towards the centerline as the thermal boundary layer grows downstream. The mean and fluctuation profiles demonstrate that the large variations in properties are concentrated close to the wall, particularly at the first heated station.

Some explanation for the appearance of 'laminarization' in the mean velocity distributions is found in Fig. 8, which shows the predicted distributions of Reynolds shear stress. This quantity can be considered to be a measure of the turbulent contribution to momentum transport. The solid lines show the DNS prediction without heating and the dashed lines give results for the heated region. All results for the heated region showed a reduction to negligible levels by $z/D \approx 14$; as far as momentum transfer is concerned, it is predicted that the flow is effectively laminarized near the wall before this station. These results indicate that the transport is molecular. Differences are in the rate of reduction of Reynolds shear stress.

The Reynolds normal stresses as represented by the root-mean-square values of the velocity fluctuations in the streamwise, radial and circumferential directions are presented in Figs. 9–11, respectively. All decrease significantly with axial distance. The streamwise component is small at the last station but the peak that is usually near $y^+$ of 15 or so, is no longer clear. The ultimate effect of the significant property variation on the radial component is very strong; there appears to be an appreciable reduction within the first three diameters. Thus, the DNS indicates that the reduction in Reynolds shear stress may be primarily a consequence of suppression of the radial component. For these conditions, the axial reduction in density due to heating leads to an acceleration parameter $K_v$ of about $4 \times 10^{-6}$, approximately the magnitude where Kline et al. (1967) observed a reduction in

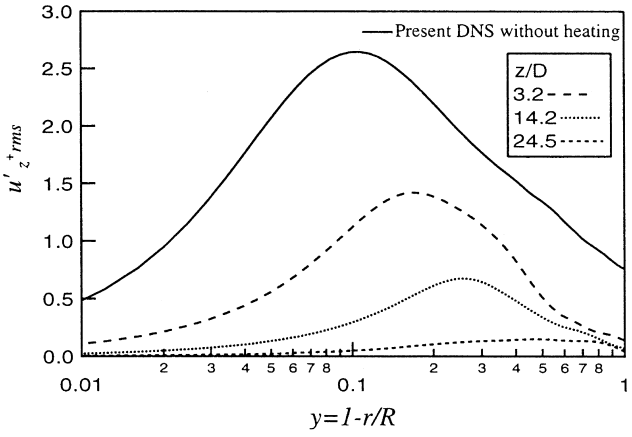


Fig. 9. Streamwise velocity fluctuations.

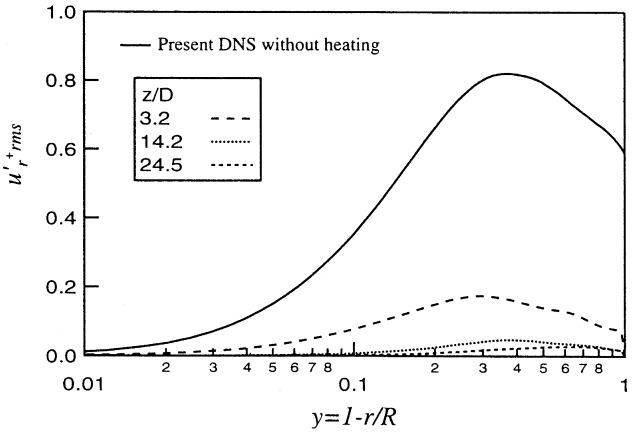


Fig. 10. Radial velocity fluctuations.

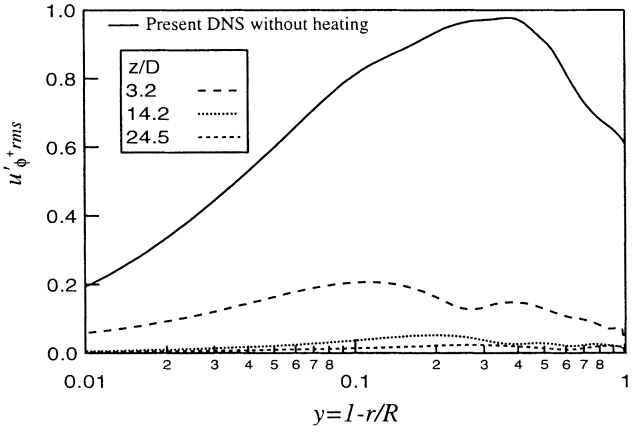


Fig. 11. Circumferential velocity fluctuations.

turbulent bursting rate near the wall for external flows with favorable streamwise pressure gradients. The magnitudes of the radial and circumferential components are roughly the same. Some streamwise turbulent fluctuations are still observable at the last station and might be detected by a hot wire anemometer (Bankston, 1970) but they would not transport much momentum, as demonstrated by the Reynolds shear stress results (Fig. 8).

The transport equation for Reynolds-averaged turbulent kinetic energy may be written as

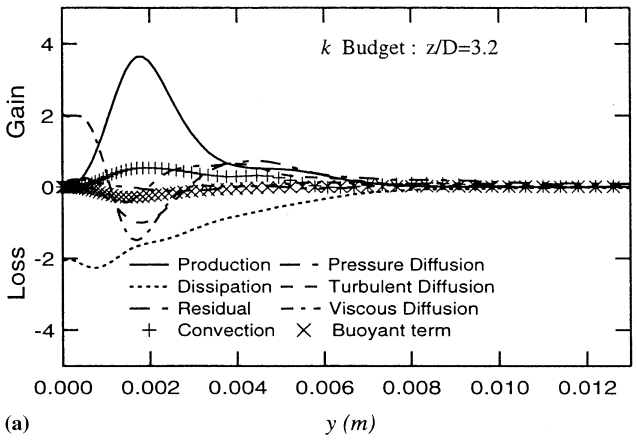


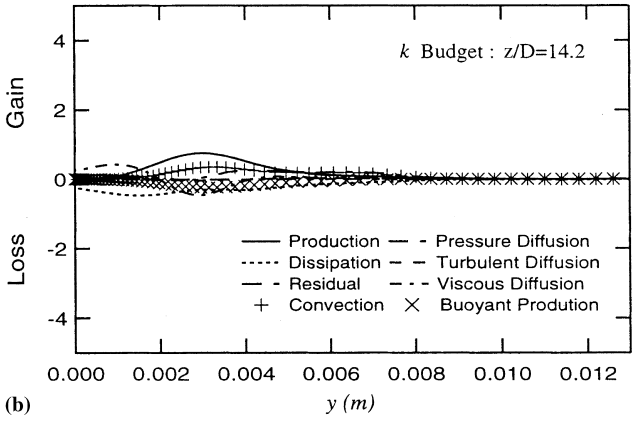


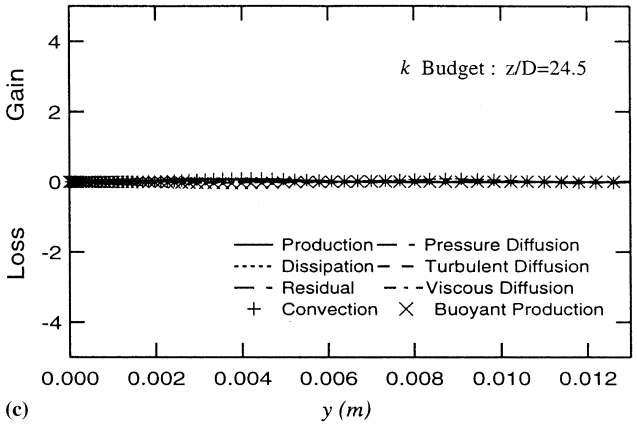


Fig. 12. Turbulent kinetic energy budget.

$$0 = \underbrace{-\overline{u_r^2}\frac{\partial U_r}{\partial r} - \overline{u_r u_z}\frac{\partial U_r}{\partial z} - \overline{u_r u_z}\frac{\partial U_z}{\partial r} - \overline{u_z^2}\frac{\partial U_z}{\partial z} - \overline{u_\phi^2}\frac{U_r}{r}}_{\text{Production}}$$
$$\underbrace{-\frac{\langle v\rangle}{\langle\rho\rangle}\overline{\frac{\partial u_i}{\partial x_j}\frac{\partial u_i}{\partial x_j}}}_{\text{Dissipation}} \underbrace{-\left(\frac{\partial \overline{pu_r}}{\partial r} + \frac{\overline{pu_r}}{r} + \frac{\partial \overline{pu_z}}{\partial z}\right)}_{\text{Pressure diffusion}}$$
$$\underbrace{-\left(\frac{\partial \overline{u_r k}}{\partial r} + \frac{\overline{u_r k}}{r} + \frac{\partial \overline{u_z k}}{\partial z}\right)}_{\text{Turbulent diffusion}} \underbrace{-U_r\frac{\partial k}{\partial r} - U_z\frac{\partial k}{\partial z}}_{\text{Convection}} \underbrace{-\frac{\overline{\rho' u_z}}{\langle\rho\rangle}}_{\text{Buoyant term}}$$
$$\underbrace{+\frac{\langle v\rangle}{\langle\rho\rangle}\left(\frac{\partial^2 k}{\partial^2 r} + \frac{1}{r}\frac{\partial k}{\partial r} + \frac{\partial^2 k}{\partial z^2}\right)}_{\text{Viscous diffusion}}, \tag{17}$$

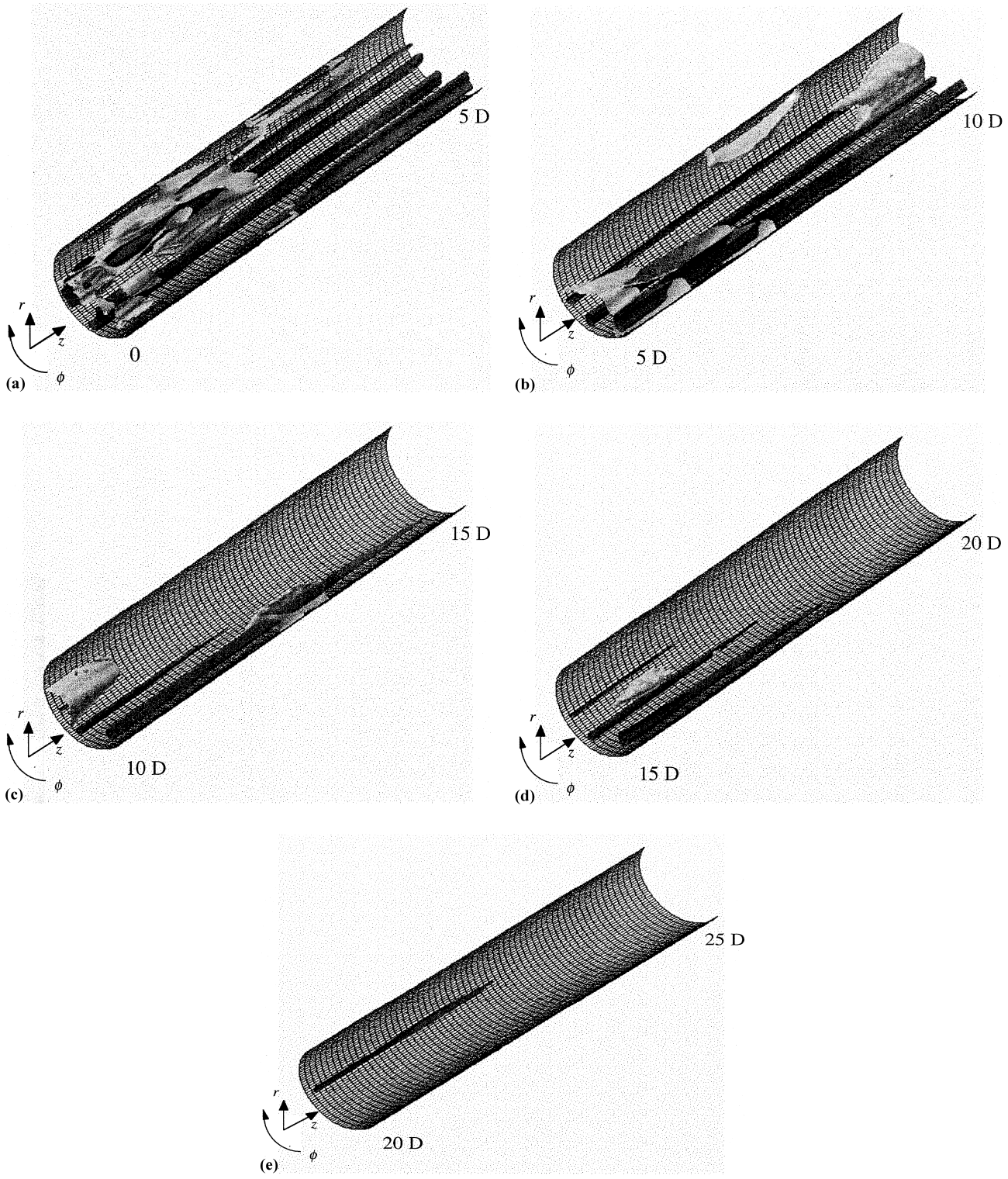


Fig. 13. Contour surface of low-pressure and low-speed regions with high heating: (a) white, $p' < -0.1$ (Pa); grey, $u'_z < -0.35$ (m/s) (at $z/D = 0$ to 5); (b) white, $p' < -0.01$ (Pa); grey, $u'_z < -0.35$ (m/s) (at $z/D = 5$ to 10); (c) white, $p' < -0.01$ (Pa); grey, $u'_z < -0.35$ (m/s) (at $z/D = 10$ to 15); (d) white, $p' < -0.01$ (Pa); grey, $u'_z < -0.2$ (m/s) (at $z/D = 15$ to 20); (e) white, $p' < -0.01$ (Pa); grey, $u'_z < -0.15$ (m/s) (at $z/D = 20$ to 25).

where $\langle\rho\rangle$ and $\langle\nu\rangle$ are the density and viscosity averaged over the circumferential direction. The budgets of turbulent kinetic energy predicted by DNS are shown in Figs. 12(a)–(c) for $z/D = 3.2$, 14.2 and 24.5, respectively. The centerline is at $y \approx 0.014$ m in this presentation. Near the entry ($z/D \approx 3$) convection and buoyant terms are observed and are very

pronounced near the location of the peak value of the production term. It is to be expected that the buoyancy effect will be strongly correlated to the distribution of temperature fluctuations, with the peaks of the convection and buoyant terms corresponding to the peak of $T_{rms}$ since the density fluctuation is caused by the temperature fluctuation. Although convection and buoyant terms exist in the budget, the overall profiles of all terms are not very different from the DNS for constant-property, fully developed flow without heating (Satake and Kunugi, 1998a); by $z/D \approx 14$ these two terms are approximately the same order as the others. Negative gradients in viscous diffusion and dissipation terms at the wall are also observed in Figs. 12(a) and (b). A similar tendency due to apparent laminarization can be observed in the DNS results for a very low Reynolds number channel by Iida et al. (1997). All terms decay in the downstream direction. By $z/D = 24.5$, all terms have nearly disappeared.

The predicted spatial evolution of structures in the flow field with strong heating is visualized sequentially in Figs. 13(a) for $z/D = 0$–5, (b) 5–10, (c) 10–15, (d) 15–20 and (e) 20–25. It should be noted that the contour levels vary in these subfigures, as indicated in the caption. The white and grey contour surfaces in the half view of the pipe represent the low-pressure and low-speed regions, corresponding to the vortical structures and wall-layer streaks, respectively. Within the first section ($z/D = 0$–5), these structures become quite different from those of pipe flow without heating (Satake and Kunugi, 1998a). However, the low-pressure regions representing the vortical structures decay rapidly beyond $z/D \approx 3$. The vortical structures disappear in this region and the low-speed streaks and their meandering become weak. One may recall that the meandering of streaks is interpreted as a dominant phase in the usual turbulence regeneration processes (Hamilton et al., 1995). Thus, in the first section of the heated region ($z/D = 0$–5), the turbulence is suppressed as a consequence of the strong heating and it is not regenerated in the downstream region. Whether this suppression fundamentally occurs due to the related property variations, acceleration, buoyancy or a combination remains a question to be answered in future studies.

## 5. Concluding remarks

New direct numerical simulations for turbulent pipe flow with strong heating were accomplished at the conditions of the experiments of Shehata and McEligot (1998). The predictive techniques have been validated by comparisons to the integral parameters and mean velocity and temperature distributions deduced from the measurements. It is shown that the resulting large thermal property change of the gas (affecting viscosity, acceleration and buoyancy) leads to a remarkable reduction of Reynolds shear stress, or 'laminarization', of the initially turbulent pipe flow. The direct numerical simulations predict that turbulent fluctuations decrease mostly after five to ten diameters and, furthermore, visualized vortical and streaky structure decay progressively in the downstream region.

## References


Akselvoll, K., Moin, P., 1995. Large eddy simulation of turbulent confined coannular jets and turbulent flow over a backward facing step, Tech. Rept. TF-63, Mech. Eng., Stanford University.

Bankston, C.A., 1970. The transition from turbulent to laminar gas flow in a heated pipe. J. Heat Transfer 92, 569–579.

Dukowicz, J.K., Dvinsky, A.S., 1992. Approximate factorization as a high order splitting for the implicit incompressible flow equations. J. Comp. Phys. 102 (2), 336–347.

Eggels, J.G.M., 1994. Direct and large eddy simulation of turbulent flow in a cylindrical pipe geometry, Ph.D. thesis, Delft University of Technology.

Ezato, K., Shehata, A.M., Kunugi, T., McEligot, D.M., 1997. Numerical predictions of transitional features of turbulent gas flows in circular tubes with strong heating, Paper FEDSM97-3304, ASME Fluids Eng. Conf., Vancouver, B.C.; Also J. Heat Transfer, 121 (1999) 546–555.

Fujii, S., Akino, N., Hishida, M., Kawamura, H., Sanokawa, K., 1991. Experimental and theoretical investigations on heat transfer of strongly heated turbulent gas flow in an annular duct. JSME Int. J. Ser II 34 (3), 348–354.

Hamilton, J., Kim, J., Waleffe, F., 1995. Regeneration mechanisms of near-wall turbulence structures. J. Fluid Mech. 287, 317–348.

Iida, O., Ohtsuka, A., Nagano, Y.,1997. The drag reduction mechanisms in the retransition of turbulent channel flow. In: Proceedings of the Second International Symposium on Turbulence, Heat and Mass Transfer. pp. 209–218.

Kawamura, H., 1979. Analysis of laminarization of heated turbulent gas using a two-equation model of turbulence. In: Proceedings of the Second International Symposium on Turbulence Shear Flow. London, pp. 18.16–18.21.

Kline, S.J., Reynolds, W.C., Schraub, F.A., Rundstadler, P.W., 1967. The structure of turbulent boundary layers. J. Fluid Mech. 30, 741–773.

Lowery, P.S., Reynolds, W.C., Mansour, N.N., 1987. Passive scalar entrainment and mixing in a forced spatially-developing mixing layer, AIAA paper, 87-0142.

McEligot, D.M., 1986. Convective heat transfer in internal gas flows with temperature-dependent properties. Adv. Transport Processes 4, 113–200.

Mikielewicz, D.P., 1994. Comparative studies of turbulence models under conditions of mixed convection with variable properties in heated vertical tubes. Ph.D. thesis, University of Manchester.

Nishimura, M., Fujii, S., Shehata, A.M., Kunugi, T., McEligot, D.M., 1997. Prediction of forced gas flows in circular tubes at high heat fluxes. In: Proceedings of the Eighth International Topical Meeting on Nuclear Reactor Thermal-hydraulics. Kyoto, pp. 294–304.

Perkins, K.R., 1975. Turbulence structure in gas flows laminarizing by heating. Ph.D. thesis, University of Arizona.

Satake, S., Kunugi, T., 1998a. Direct numerical simulation of turbulent pipe flow. Bulletin, JSME 64, 65–70 (in Japanese).

Satake, S., Kunugi, T., 1998b. Direct numerical simulation of an impinging jet into parallel disks. Int. J. Num. Meth. Heat Fluid Flow 8, 768–780.

Satake, S., Kunugi, T., 1998c. Direct numerical simulation of turbulent pipe flow with non-uniform surface heat flux. Thermal Sci. Eng. 6 (2), 1–7 (in Japanese).

Shehata, A.M., McEligot, D.M., 1998. Mean turbulence structure in the viscous layer of strongly heated internal gas flows: Measurements. Int. J. Heat Mass Transfer 41, 4297–4313.

Spalart, P.R., Moser, R.D., Rogers, M.M., 1991. Spectral methods for the Navier–Stokes equations with one infinite and two periodic directions. J. Comp. Phys. 96, 297–324.

Takase, K., Hino, R., Miyamoto, Y., 1990. Thermal and hydraulic tests of standard fuel rod of HTTR with HENDEL. J. Atomic Energy Soc. Jpn. 32–11, 1107–1110 (in Japanese).

Torii, S., Shimizu, A., Hasegawa, S., Higasa, M., 1993. Numerical analysis of laminarizing circular tube flows by means of a Reynolds stress turbulence model. Heat Transfer – Japanese Res. 22, 154–170.

Torii, S., Yang, W.-J., 1997. Laminarization of turbulent gas flow inside a strongly heated tube. Int. J. Heat Mass Transfer 40, 3105–3117.

Verzicco, R., Orlandi, P., 1996. A finite-difference scheme for three-dimensional incompressible flows in cylindrical coordinate. J. Comp. Phys. 123, 402–414.